ELSEVIER

Journal of Fluids and Structures 24 (2008) 200–211

JOURNAL OF FLUIDS AND STRUCTURES

www.elsevier.com/locate/jfs

Theoretical and experimental studies on the aerodynamic instability of a two-dimensional circular cylinder with a moving attachment

M. Gu*, L. Huang

State Key Laboratory Disaster Reduction in Civil Engineering, Tongji University, Shanghai 200092, China

Received 17 November 2005; accepted 4 August 2007
Available online 8 November 2007

Abstract

Rain–wind induced vibration of cables in cable-stayed bridges is a worldwide problem of great concern. The effect of the motion of water rivulets on the instability of stay cables has been recognized as one of the mechanisms of this complex phenomenon. In order to investigate how the motion of rivulets affects the unstable vibration of cables without considering the effects of axial flow and axial vortex, a real three-dimensional cable was modeled as a two-dimensional circular cylinder, around which an attachment representing the rivulet can move. This could also be regarded as a new kind of two-dimensional 2-dof dynamic system. This paper studies the aerodynamic instability of the system theoretically and experimentally. Equations governing the motions of the cylinder and the attachment are first established. The Lyapunov stability criterion is applied to the equations of motion to derive the criterion for the unstable balance angle of the attachment. Moreover, a new two-dimensional 2-dof cable model system with a movable attachment is designed and tested in a wind tunnel. Parametric studies are carried out to investigate the effects of major factors such as wind speed, frequency and damping of the dynamic system on the unstable balance angle of the rivulet attachment. Theoretical and experimental results match well. These results may be valuable in elucidating the mechanism of rain–wind induced vibration of stay cables.

Keywords: Two-dimensional circular cylinder; Stay cable; Rain–wind induced vibration; Moving rivulet; Unstable balance angle

1. Introduction

The literature over the past 20 years contains reports of excessive and unanticipated vibration of cables in cable-stayed bridges under the simultaneous occurrence of wind and rain (Hikami and Shiraishi, 1988; Ohshima and Nanjo, 1987; Matsumoto et al., 2003; Matsumoto, 1998; Pacheco and Fujino, 1993; Main and Jones, 1999; Persoon and Noorlander, 1999). Wind–rain induced cable vibrations have also been observed in two cable-stayed bridges recently built in Shanghai (Gu et al., 1998) and in Nanjing (Shi, 2000), which have main spans of 602 and 608 m, respectively. Rain–wind induced cable vibration has become of great concern in the bridge and wind engineering communities.

*Corresponding author. Tel./fax: +81 21 65981210.
E-mail address: minggu@mail.tongji.edu.cn (M. Gu).

0889-9746/$ - see front matter
doi:10.1016/j.jfluidstructs.2007.08.001

In order to investigate the mechanism of this phenomenon, field measurements (Hikami and Shiraishi, 1988; Ohshima and Nanjo, 1987; Matsumoto, 1998; Main and Jones, 1999; Persoon and Noorlander, 1999; Shi, 2000), wind tunnel simulation tests (Matsumoto et al., 1992, 1995; Flamand, 1995; Bosdogianni and Olivari, 1996; Gu et al., 2002; Gu and Du, 2005), and theoretical analyses (Yamaguchi, 1990; Gu and Lu, 2001; Wilde and Witkowski, 2003; Geurts and Staalduinen, 1999; Xu and Wang, 2003a; Cao et al., 2003) have been conducted by researchers and engineers around the world. In wind tunnel simulation tests, there are two main approaches to simulate a rivulet on a cable section model: one is to spray water onto the surface of the cable model to form a rivulet (Matsumoto et al., 1995; Gu and Du, 2005), and the other is to place an artificial rivulet on the cable surface (Gu et al., 2002; Yamaguchi, 1990; Gu and Lu, 2001). Many recent studies have indicated that the movement of the upper rivulet around the cable surface could be responsible for the rain–wind induced vibration of stayed cables (Gu et al., 1998, 2002; Gu and Du, 2005; Yamaguchi, 1990; Verwiebe and Rucheweyh, 1998; Matsumoto, 2005). In a previous paper, Matsumoto (2005), adopted unsteady aerodynamic forces, which were expressed by aerodynamic derivatives $H_i^*(i = 1, 2, 3, 4)$ to study the aerodynamic damping and instability. Other researchers adopted a quasi-steady state assumption of aerodynamic force for the rain–wind induced vibration (Yamaguchi, 1990; Gu and Lu, 2001; Xu and Wang, 2003a); and furthermore, some studies have also suggested that the rain–wind induced vibration of stay cables may be similar to classical galloping (Gu and Lu, 2001). In addition, Matsumoto et al. discovered that stay cables vibrate at higher reduced wind speeds, such as 20, 40, 60 and 80, under rain–wind conditions or under only wind conditions from field measurements (Matsumoto and Shirato, 2003) and wind tunnel tests (Matsumoto et al., 2001). From these observations, the authors proposed axial flow and axial vortices as other possible mechanisms for rain–wind induced vibration (Matsumoto and Shirato, 2003; Matsumoto et al., 2001; Zuo et al., 2004). Nevertheless, the mechanism of rain–wind induced vibration of stay cables remains unclear. Here, we apply the quasi-steady assumption to see if this approach is a feasible way to solve the problem of rain–wind induced vibration.

By understanding the possible mechanisms of rivulet motion, a new two-dimensional 2-dof dynamic system is modeled and its aerodynamic instability is theoretically and experimentally studied to investigate how the motion of rivulets affects the unstable vibration of the cables, without considering the effects of axial flow and axial vortex. In the model, a real three-dimensional cable is simply modeled as a two-dimensional circular cylinder around which an attachment representing the rivulet can move. If a three-dimensional cable model were adopted for this study, it would have been difficult to distinguish whether the motion of the upper rivulet or axial flow was the main contributor to instability. Although the two-dimensional 2-dof model does not correspond to the actual situation of rain–wind induced vibration of cables, it could still be adopted to investigate the characteristics of rain–wind induced vibration of cables at a unique angle of view. Therefore, in this paper, to remove the effect of axial flow and axial vortices on the unstable motion of the cables and to simplify the analysis, it is assumed that the rivulet could form on the cable surface at a zero wind yaw angle, and thus only a two-dimensional cable is considered. This model could also be regarded as a new kind of 2-dof dynamic system. Based on this idea, equations governing the motion of the cylinder and the attachment are first established. The Lyapunov stability criterion is then applied to the equations of motion to derive the criterion for the unstable balance angle of the rivulet attachment. A new two-dimensional 2-dof circular cylinder with a movable attachment is designed and tested in a wind tunnel.

2. Equations governing motions of the cable and rivulet

2.1. Basic assumptions

The phenomenon of rain–wind induced vibration of cables is very complex. In order to simplify the analysis, some appropriate assumptions are made as in previous studies.

(i) In order to only consider the effects of the motion of the rivulet on the unstable motion of cables, the axial flow and axial vortices along the cable will not be taken into account in this analysis.
(ii) Only the upper rivulet will be taken into account in the following analysis. Previous studies (Gu et al., 2002; Yamaguchi, 1990) have indicated that the lower rivulet is generally located behind the lower separation point and thus has little effect on wind pressure distributions and aerodynamic forces, while the upper rivulet has a significant effect on aerodynamic forces.
(iii) The quasi-steady state assumption will be applied in the present analysis. The Strouhal number of a two-dimensional circular cylinder with a diameter of 10–20 cm in a sub-critical Re number range is around 0.2; and the rain–wind induced vibration of cables generally takes place at lower frequencies. Therefore, if a cable vibrates with the above

parameters caused by the Karman vortex excitation, the excitation wind speed will be much lower than the onset wind speed of rain–wind induced vibration. That is to say, the frequency of the rain–wind induced vibration generally differs greatly from the frequency of the Karman vortex excitation. Moreover, the effects of axial flow and axial vortices are not taken into account, as indicated above. Furthermore, although some researchers have pointed out that the unsteady force on a circular cylinder with an artificial rivulet cannot be expressed by quasi-steady state analysis (Matsumoto, 2005), many researchers (Yamaguchi, 1990; Gu and Lu, 2001; Xu and Wang, 2003a) have also adopted the quasi-steady assumption to calculate the aerodynamic force for the rain–wind induced vibration of cables. In view of these observations, the quasi-steady assumption will be applied in the present study even if this approach may be an imperfect way to describe rain–wind induced vibration.

2.2. Analysis of the motion of the cable and rivulet

Fig. 1 shows a schematic drawing of the motion of the two-dimensional 2-dof dynamic system. In this figure, y and $\dot{y}$ denote the vibration displacement and velocity of the cable, respectively; β_0 denotes the balance angle of attachment representing the rivulet under the actions of its own gravitational force, the surface tension between the rivulet and the cable surface, and wind forces. The balance angle of attachment corresponding to the aerodynamic instability of the cylinder model is defined as the "unstable balance angle"; and γ denotes the instantaneous angle of the rivulet's motion relative to β_0. From this figure, the relative wind speed, U_{rel}, can be derived as

$$U_{\text{rel}} = \sqrt{U^2 + \dot{y}^2}, \tag{1}$$

and the included angle between U_{rel} and U is

$$\alpha = \arctan\frac{\dot{y}}{U}. \tag{2}$$

2.3. Analysis of forces for the cable and rivulet

The radius, mass, stiffness and damping coefficient of the two-dimensional 2-dof cable system are denoted by R, M, K and C, respectively. The forces acting on the cable and the rivulet can be found in Fig. 2. The forces acting on the cable are inertial forces, $M\ddot{y}$, of the cable itself due to its motion; damping force, $C\dot{y}$; elastic force, Ky; wind forces, i.e., drag force, F_D, and lift force, F_L; and the tangential and normal components of the force from the rivulet, F_1 and F_2. The forces acting on the rivulet are the gravity of the rivulet itself, mg, and the tangential and normal projections of the aerodynamic force, P^{τ} and P^{n}. Du (2004) made measurements on the wind pressures of a cable model and the attached artificial rivulet, and the results showed that P^{n} is very small. F_1 and F_2 are the tangential and normal components of the surface tension between the rivulet and the cable surface. In fact, the forces acting on the cable model caused by the rivulet are much smaller than the forces of the cable model itself and have almost no effect on the cable motion, and they are therefore omitted from the equation of motion of the cable. The inertial forces of the rivulet can be decomposed into $m\ddot{y}$, $mR\ddot{\gamma}$ and $mR\dot{\gamma}^2$. In addition, let $\theta = \beta_0 + \gamma - \alpha$.

2.4. Equations governing the motion of the cable and rivulet

Based on the above analysis, the force balance equations for the cable and rivulet can be derived based on the D'Alembert principle as follows:

$$M\ddot{y} + C\dot{y} + Ky = F_y(\theta, \alpha), \tag{3}$$

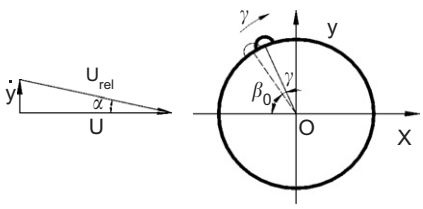

Fig. 1. Schematic diagram describing the motion of the cable and rivulet.

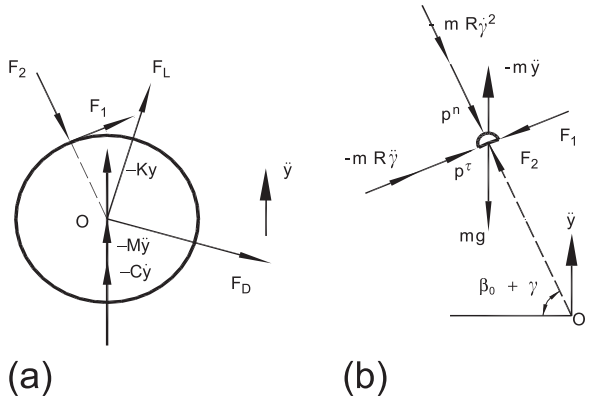

Fig. 2. Schematic diagram of forces acting on the cable and rivulet; (a) cable and (b) rivulet.

$$m(\ddot{y}+g)\cos(\beta_0+\gamma)-P^{\tau}+mR\ddot{\gamma}+F_1=0, \tag{4}$$

where $F_y(\theta,\alpha)$ is the aerodynamic force in the y-direction, which will induce vibration of the cable and is composed of the components $F_D(\theta)$ and $F_L(\theta)$ as follows:

$$F_y(\theta,\alpha)=\rho RU^2C_y(\theta,\alpha)=F_L(\theta)\cos\alpha-F_D(\theta)\sin\alpha, \tag{5}$$

where ρ is the mixed density of air and rain.

Based on the quasi-steady assumption, $F_D(\theta)$ and $F_L(\theta)$ can be written as

$$F_D(\theta)=\rho RU_{\mathrm{rel}}^2C_D(\theta), \tag{6}$$

$$F_L(\theta)=\rho RU_{\mathrm{rel}}^2C_l(\theta), \tag{7}$$

where $C_D(\theta)$ and $C_L(\theta)$ are the drag and lift force coefficients, respectively.

From Eqs. (5), (6) and (8), $F_y(\theta)$ can be written as

$$F_y(\theta,\alpha)=\rho U^2R[-C_D(\theta)\tan\alpha+C_L(\theta)]\frac{1}{\cos\alpha}. \tag{8}$$

Comparing Eqs. (5) and (8), the aerodynamic force coefficient $C_y(\theta)$ can be expressed as

$$C_y(\theta,\alpha)=[-C_D(\theta)\tan\alpha+C_L(\theta)]\frac{1}{\cos\alpha}. \tag{9}$$

Letting $\tau=\omega t$ and $\eta=y/R$, the nondimensional equations governing the motion of the cable and rivulet can further be written as

$$\eta''+2\zeta\eta'+\eta=\varepsilon\frac{1}{\pi\mu_r^2}C_y(\theta,\alpha), \tag{10}$$

$$\gamma''+\left(\eta''+\frac{g}{R\omega^2}\right)\cos(\beta_0+\gamma)+F_1=\frac{P^{\tau}}{mR\omega^2}, \tag{11}$$

where $\omega=\sqrt{K/M}$ is the natural circular frequency of the cable, generally ranging from 2 to 18; ζ is the damping ratio of the cable system; $\delta=m/M$ is the mass ratio between the rivulet and the cable; R is the radius of the cable; $\varepsilon=\pi R^2\rho/M$; $\mu_r=R\omega/U$; and η' and γ' denote the derivatives of η and γ, respectively, with respect to nondimensional time, τ.

3. Criterion for the unstable motion of the cable

3.1. Taylor expansion of $F_y(\theta)$

In order to derive the criterion for the unstable motion of the cable, $F_y(\theta)$ is expanded into a Taylor's series at $\alpha=\gamma=0$, and the items higher than first order are neglected. Additionally, $\alpha=\tan^{-1}(\dot{y}/U)\approx\dot{y}/U=\mu_r\,\eta'$ when $\alpha\approx 0$ and $\gamma\approx 0$. Thus,

$$C_y\approx C_L(\theta)-\mu_r\left[C_D(\theta)+\frac{\partial C_L(\theta)}{\partial\alpha}\right]\eta'+\frac{\partial C_L(\theta)}{\partial\gamma}\gamma. \tag{12}$$

When the balance angle β_0 is fixed at a constant value and $\alpha\approx\gamma\approx 0$, $\partial C_L(\theta,\beta_0)/\partial\alpha=\partial C_L(\theta,\beta_0)/\partial\gamma=\partial C_L(\theta,\beta_0)/\partial\theta$. Thus,

$$C_y\approx C_L(\theta)-\mu_r\left[C_D(\theta)+\frac{\partial C_L(\theta,\beta_0)}{\partial\theta}\right]\eta'+\frac{\partial C_L(\theta,\beta_0)}{\partial\theta}\gamma. \tag{13}$$

In Eq. (13), the first item on the right-hand side, $C_L(\beta_0)$, is the mean lift coefficient and cannot produce the vibration of the cable, so it is not considered in the following analysis. The second item is the aerodynamic force induced by the motion of the cable, which is similar to the classical galloping force coefficient; and the third item $[\partial C_L(\beta_0)/\partial\theta]\gamma$ is the aerodynamic force coefficient induced by the motion of the upper rivulet, which depends on the balance angle, β_0, and the instantaneous angle, γ, of the upper rivulet.

3.2. Criterion for stability of the cable

It is difficult to obtain the precise value of P^τ in Eq. (11) from the present analysis, so the vibration amplitude of the rivulet, γ, cannot be obtained precisely. Therefore, the characteristics of the instability of stay cables will be investigated theoretically based only on the equation of motion of the cable, i.e., Eq. (10), making an assumption of the vibration amplitude of the rivulet.

Applying the Lyapunov stability criterion to Eq. (13), the criterion for the unstable motion of the cable can be derived. Substituting Eq. (13) without the $C_L(\theta)$ term into Eq. (10) leads to the equation of motion of the cable in state space style as

$$\begin{cases} x_1'=x_2,\\ x_2'=-x_1-\left\{2\zeta+\varepsilon\dfrac{1}{\pi\mu_r}\left[C_D(\beta_0)+\dfrac{\partial C_L(\theta,\beta_0)}{\partial\theta}\right]\right\}x_2+\varepsilon\dfrac{1}{\pi\mu_r^2}\dfrac{\partial C_L(\theta,\beta_0)}{\partial\theta}\gamma, \end{cases} \tag{14}$$

where $x_1=\eta$ and $x_2=x_1'=\eta'$.

The energy function is $E=\frac{1}{2}x_1^2+\frac{1}{2}x_2^2$, and the Lyapunov function V is the integration of the energy function over a period of 2π:

$$V=\int_\tau^{\tau+2\pi}E\,\mathrm{d}\tau. \tag{15}$$

The derivative of E with respect to nondimensional time τ is

$$\frac{\mathrm{d}E}{\mathrm{d}\tau}=-\left\{2\zeta+\varepsilon\frac{1}{\pi\mu_r}\left[C_D(\theta,\beta_0)+\frac{\partial C_L(\theta,\beta_0)}{\partial\theta}\right]\right\}x_2^2+\varepsilon\frac{1}{\pi\mu_r^2}\frac{\partial C_L(\theta,\beta_0)}{\partial\theta}x_2\gamma. \tag{16}$$

Thus,

$$\frac{\mathrm{d}V}{\mathrm{d}\tau}=-\left\{2\zeta+\varepsilon\frac{1}{\pi\mu_r}\left[C_D(\theta,\beta_0)+\frac{\partial C_L(\theta,\beta_0)}{\partial\theta}\right]\right\}\int_\tau^{\tau+2\pi}x_2^2\,\mathrm{d}\tau+\varepsilon\frac{1}{\pi\mu_r^2}\frac{\partial C_L(\theta,\beta_0)}{\partial\theta}\int_\tau^{\tau+2\pi}\gamma x_2\,\mathrm{d}\tau. \tag{17}$$

According to the Lyapunov stability criterion, the cable motion is stable for $\mathrm{d}V/\mathrm{d}\tau\leqslant 0$ and unstable for $\mathrm{d}V/\mathrm{d}\tau>0$. Furthermore, the unstable balance angle of the rivulet can be derived based on the following assumptions: (i) both the cable and rivulet vibrate in simple harmonic ways; (ii) the rivulet vibrates at the same frequency as that of the cable, in a fixed phase.

Cosentino et al. (2003) measured rivulet motions using a new technique and pointed out that the water rivulet moved in a harmonic way, and that the main frequency of the water thickness measurement was the same as the cable vibration frequency. The two assumptions adopted in that paper coincide with the above finding.

The above two assumptions mean that

$$x_1 = A\sin\tau, \quad x_2 = A\cos\tau, \quad \gamma = -\bar{B}\sin(\tau+\varphi), \tag{18}$$

where A and $\bar{B}$ are the amplitudes of x_1 and γ, respectively, which are both positive values. The negative sign before $\bar{B}$ means that the phase difference in motion between the cable and the rivulet is about 180°, with a smaller variation expressed by φ. This may be due to the inertial force caused by the acceleration of the cable that induces a motion of the attachment in reverse of the cable model's motion. Matsumoto (2005) pointed out that the instability is quite sensitive to phase. This can also be found from the present theoretical model. However, it is difficult to determine the actual phase in a rain–wind induced vibration phenomenon. The basis of the above assumption could also be found from the theoretical models of Gu and Lu (2001), Verwiebe and Rucheweyh (1998), Ruscheweyh (1999) and Xu and Wang (2003b).

Substituting Eq. (21) into (20) leads to

$$\frac{\mathrm{d}V}{\mathrm{d}\tau} = -\pi AB\left\{\frac{A}{B}\left[2\zeta + \varepsilon\frac{1}{\pi\mu_r}\left(C_D(\theta) + \frac{\partial C_L(\theta,\beta_0)}{\partial\theta}\right)\right] + \varepsilon\frac{1}{\pi\mu_r^2}\frac{\partial C_L(\theta,\beta_0)}{\partial\theta}\right\}, \tag{19}$$

where $B = \bar{B}\sin\varphi$. It is further assumed that the value of $B = \bar{B}\sin\varphi$ is positive.

Thus, the criterion for the unstable motion of the cable finally derived as

$$\Delta = \frac{A}{B}\left[2\zeta + \varepsilon\frac{1}{\pi\mu_r}\left(C_D(\theta) + \frac{\partial C_L(\theta,\beta_0)}{\partial\theta}\right)\right] + \varepsilon\frac{1}{\pi\mu_r^2}\frac{\partial C_L(\theta,\beta_0)}{\partial\theta} < 0. \tag{20}$$

The unstable balance angle, β_0 corresponding to the unstable motion of the cable can be found using Eq. (20).

In Eq. (20), A/B is the amplitude ratio of the cable and rivulet, which is permanently greater than or equal to zero. In fact, the value of A/B is difficult to predict precisely for a real cable because P^{τ} in Eq. (14) is difficult to obtain accurately, as mentioned before. Therefore, the criteria for the two limit conditions of A/B are further derived as follows.

(1) $A/B \to \infty$.

$A/B \to \infty$ means $B \to 0$, that is to say, the rivulet is motionless. This situation corresponds to galloping of the cable. The range of the unstable balance angle can be found from

$$2\zeta + \varepsilon\frac{1}{\pi\mu_r}\left(C_D(\theta) + \frac{\partial C_L(\theta,\beta_0)}{\partial\theta}\right) < 0. \tag{21}$$

The above equation is the same as the criterion for classical galloping, i.e., the well-known Den Hartog galloping criterion.

(2) $A/B \to 0$.

$A/B \to 0$ means that the nondimensional amplitude of the cable is much smaller than that of the rivulet. The criterion for this condition can be derived from Eq. (20) as

$$\frac{\partial C_L(\theta,\beta_0)}{\partial\theta} < 0. \tag{22}$$

4. Numerical computations

As an example, the unstable motion of a two-dimensional cable with a movable rivulet attachment is computed with the above criteria to investigate the effects of the main factors on the unstable balance angle of the rivulet. The parameters of the cable are taken as: diameter of 10 cm; mass density of 7800 kg/m^3; frequency of 1 Hz; damping ratio of zero. In addition, the mixed density of air and rain is assumed to be 1.5 kg/m^3, with a wind speed of 10 m/s.

The lift and drag coefficients of a cable model (diameter of 100 mm) with an artificial rivulet (a bow-shaped rivulet with a height of 6 mm and a base breadth of 10 mm) given in Gu and Lu (2001) are used in the present study. The aerodynamic force coefficients are shown in Fig. 3. In fact, the same aerodynamic force values were used in a previous study (Wilde and Witkowski, 2003). As shown in the figure, there are sudden changes in the lift and drag coefficients within a range from about 38° to 48°, which is the galloping unstable zone.

As pointed out by the authors (Gu et al., 2002) and other researchers (Bosdogianni and Olivari, 1996), the position of the rivulet on the cable surface, rather than shape and size of the rivulet, is the most important factor for aerodynamic forces that act on the cable, and thus rain–wind induced vibration.

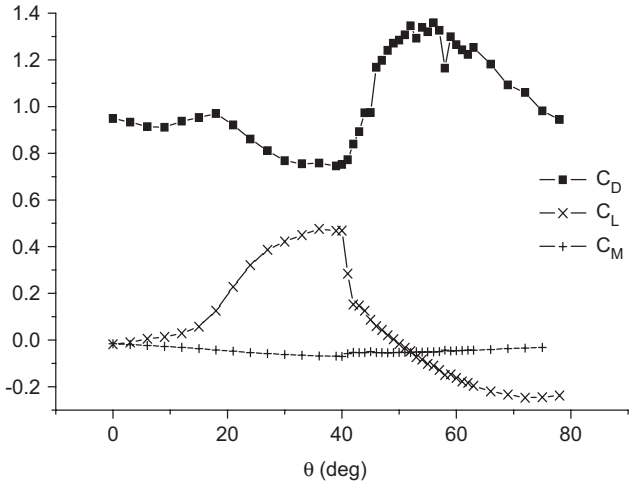

Fig. 3. Aerodynamic force coefficients of a cable with an upper artificial rivulet (Gu and Lu, 2001).

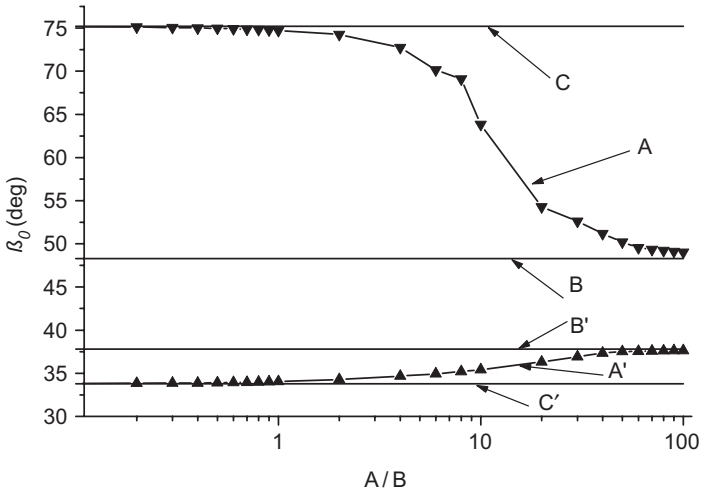

Fig. 4. Unstable balance angle versus A/B (from computation).

4.1. Variation of the unstable balance angle with A/B

Fig. 4 shows the range of variation of the unstable balance angle of the rivulet with A/B. The curves A and A′ in Fig. 4 are computed with Eq. (20), and the zone between them corresponds to an unstable zone for different values of A/B. Accordingly, the curves B and B′ are computed with Eq. (21), and the curves C and C′ are obtained with Eq. (22). The zone between curves B and B′ corresponds to the unstable zone of the galloping of the cable, and that between curves C and C′ corresponds to the upper limit of the unstable state, as mentioned above. The unstable zone between A and A′ varies gradually from the upper boundaries (C and C′) to the lower boundaries (B and B′) with increasing values of A/B. This reveals that the range of unstable balance angles of the rivulet of a cable with a movable upper rivulet could be much wider than that of unstable galloping of a cable with a fixed rivulet. From these results, it could be further deduced that the motion of the rivulet around the cable surface causes a large-amplitude vibration of cables that occur more easily than galloping. This is consistent with the result reported in Gu and Lu (2001).

4.2. Effect of damping of the cable

The parameters of the cable and rivulet are taken to be the same as those in Section 4.1, except $A/B = 5$ and there are 12 different cable damping ratios ranging from 0.4% to 1.4%. The variations in the range of unstable balance angles of

the rivulet with the damping ratio are computed with Eq. (20) and shown in Fig. 5. It can be seen from the figure that the unstable balance angle decreases with increased damping, meaning that rain–wind induced vibration does not easily occur with larger damping. This coincides with the results from field observations and wind tunnel tests (Shi, 2000; Gu and Du, 2005).

4.3. Effect of the frequency of the cable

For this investigation, the damping ratio of the cable is assumed to be 0.4%, the frequency varies from 0.5 to 3.5 Hz, and the other parameters are identical to those in Section 4.1. Fig. 6 presents the variation of an unstable balance angle with the cable frequency. The figure indicates that the range of the unstable balance angle decreases with increasing frequency. When the cable frequency reaches about 1.5 Hz, the unstable range becomes very small.

5. Wind tunnel experiment

In order to verify the above theoretical model, a new two-dimensional 2-dof dynamic system model representing the two-dimensional cable-rivulet system was designed and built. The test was performed in the TJ-1 Boundary Layer Wind Tunnel at Tongji University, with working dimensions of 1.8 m high and 1.8 m wide. The results of the tests were then compared with the theoretical predictions.

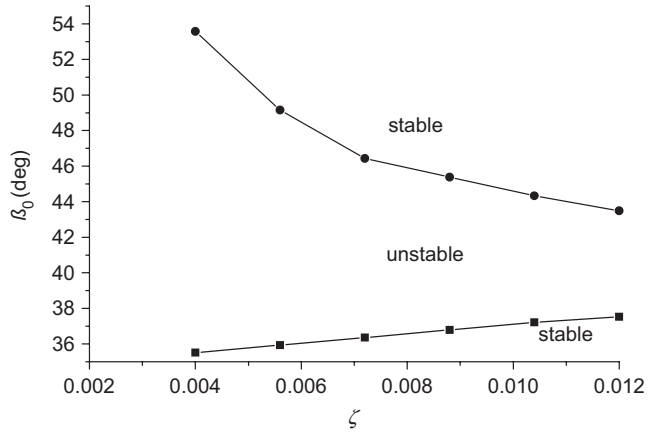

Fig. 5. Effect of damping on the unstable balance angle (from computation).

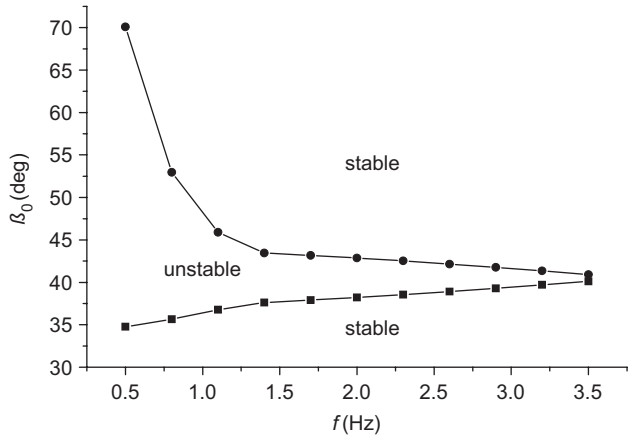

Fig. 6. Effect of frequency on the unstable balance angle (from computation).

5.1. New cable model system and testing conditions

In contrast to cable models with a fixed upper artificial rivulet used in previous studies, the new cable model system has a movable artificial upper rivulet. Fig. 7 shows the schematic diagram of the cable model system. The cable model, with a weight of 2.3 kg, is a hollow PVC tube with an outside diameter of 110 mm, a wall thickness of 3 mm and a length of 1.2 m; the movable artificial rivulet, with a weight of 0.096 kg, is a hollow aluminum tube with an outside diameter of 6 mm, a wall-thickness of 1 mm and a length of 1.26 m. As indicated above, the position of the rivulet on the cable surface, rather than shape and size of the rivulet, is the most important factor for the aerodynamic force. The figure-8 shaped attachment could thus be useful in the present test. The ends of the cable model tube were sealed with two circular wooden blocks, on which the movable attachment system representing the artificial rivulet, including two steel axles, two bearings, two connecting bars, two springs and the artificial rivulet, were mounted. The artificial rivulet can vibrate around the cable model. The frequencies of the cable model and the movable artificial rivulet are 1.47 and 1.4 Hz, respectively. It is difficult to measure precisely the damping of the rivulet, but the value is very small, about 2–4‰. The interval between the artificial rivulet and cable model can be carefully adjusted using a thin copper sheet with a thickness of 0.4 mm. The artificial rivulet must not touch the cable model during its vibration process, and the interval must be as small as possible. The interval in this system is about 0.4–0.5 mm.

The variable parameters for the test were wind velocity (4–13 m/s), the damping ratio of the cable model (0.1%, 0.53%, 1.06% and 1.7%) and the initial angle of the rivulet (10°, 20°, 30°, 35°, 40°, 43°, 45°, 47°, 50° and 60°). Two mini-accelerometers were mounted on the cable model and two on the rivulet model to detect vibration signals. The recording duration for each testing condition was 106 s at a sampling frequency of 308 Hz. All the balance angles were also recorded during the test.

5.2. Main experimental results and a comparison with the theoretical results

The unstable balance angle is first investigated for a fixed artificial rivulet on the cable model. The results show that the range of the unstable balance angle of the rivulet is from 38° to about 46°, which indicates a classical galloping phenomenon. This meets the expectation in Eq. (21).

When the rivulet is movable, the artificial rivulet will arrive at a certain balance angle from its initial position at a certain wind speed. The effects of the parameters of wind speed and damping ratio of the cable model on the unstable balance angle of the rivulet are discussed below.

5.2.1. Effect of wind speed

Fig. 8 presents the effect of wind speed on the unstable balance angle. The empty circles in this figure represent the test results, and the solid lines denote the contours of the unstable balance angles from the test. As can be seen from the figure, the unstable balance angle range becomes larger with increasing wind speed. A previous study (Gu and Lu, 2001) proposed an explanation for the mechanism of rain–wind induced vibration of cables by suggesting that there might be a "danger zone" of the instantaneous angle of the upper rivulet. When the upper rivulet vibrates from its balance angle to the "danger zone", the vibration amplitudes of the rivulet and the cable suddenly increase. This "danger zone" corresponds to the zone of the galloping force coefficient with a negative slope, i.e., the galloping unstable zone. The balance angle of the rivulet corresponding to the unstable motion of the cable is the *unstable balance angle* defined in the present paper. The previous analysis (Gu and Lu, 2001) indicated that the unstable balance angle for a cable with a movable rivulet has a wider range than that of a cable with a fixed rivulet. In particular, it is easier for the rivulet to arrive at the "danger zone" from its balance angle at higher wind speeds than at lower wind speeds, meaning that the range of the unstable balance angle is widened for higher wind speeds.

5.2.2. Effect of damping of the cable

Fig. 9 shows the effect of cable damping on the region of the unstable balance angle. The unstable region becomes smaller with an increase in damping, which is similar to the numerical results shown in Fig. 5, wind tunnel tests (Gu and Du, 2005) and field measurements (Shi, 2000).

5.2.3. Comparison of theoretical and test results

Several groups of cable models with typical damping ratios (0.1%, 0.53%, 1.06% and 1.7%) and initial rivulet angles (10°, 20°, 30° and 40°) were tested further to compare theoretical and test results to verify the present theoretical model. The parameters for the computation were the same as those for the wind tunnel test. In addition, the aerodynamic forces shown in Fig. 3 (Gu and Lu, 2001) were also adopted for this computation. Although the diameter (110 mm) of the cable model

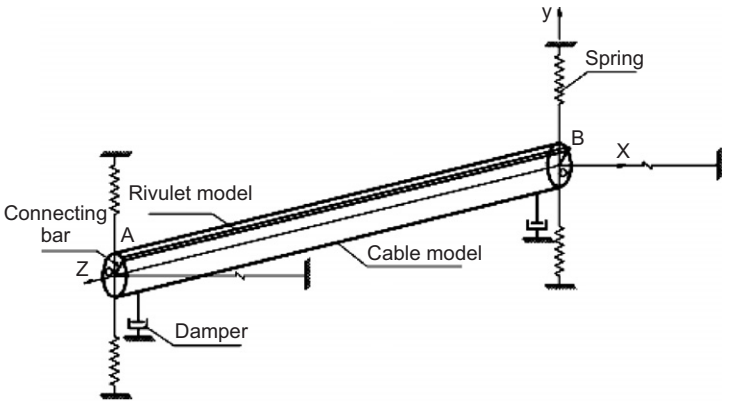

Fig. 7. Schematic diagram of the experimental set-up.

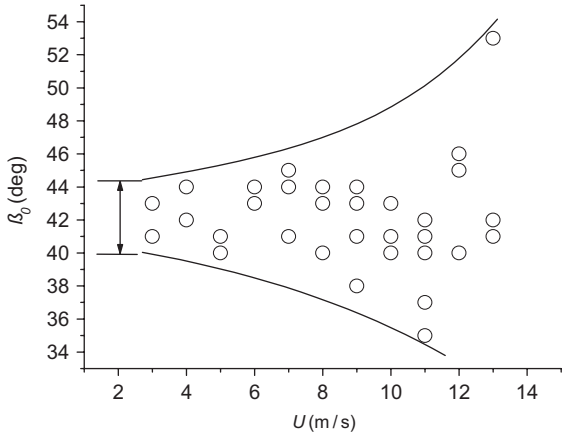

Fig. 8. Unstable balance angle versus wind speed (experimental results).

and the size of the artificial rivulet for the present test are somewhat different from the diameter (100 mm) and size of the rivulet in Gu and Lu (2001), the aerodynamic forces given in Fig. 3 could still be adopted for the present computation. This is based on the conclusions given in Gu et al. (1998) and Gu and Lu (2001) and other literature which suggest that small differences in the sizes of cables and rivulets have almost no effect on the characteristics of rain–wind induced vibration of the cables. All of the comparisons show the same tendency. Fig. 10 shows one of the comparison groups ($\zeta = 0.017$; initial angle $= 10^\circ$; wind speed $= 5-11$ m/s), together with the upper and lower boundaries of the unstable balance angle computed with Eq. (20). The figure shows clearly that the unstable balance angles of the rivulet for different wind speeds are within the boundaries calculated from the theoretical formulas. Moreover, the experimental results also show that higher wind speeds widen the range of unstable balance angles, as indicated before.

6. Concluding remarks

The effects of rivulet motion on the unstable vibration of stay cables were investigated through theoretical and experimental studies on the aerodynamic instability of a two-dimensional circular cylinder with a moving attachment. The Lyapunov stability criterion was applied to the dynamic system to derive the criterion for the balance angle of the upper rivulet corresponding to an unstable vibration of the cable. The criterion is composed of two parts: one corresponds to the criterion for classical galloping, i.e., the well known Den Hartog galloping criterion, and the other part corresponds to the rivulet motion. Numerical computations were performed to investigate the effects of the cable frequency and damping on the characteristics of the unstable balance angle. In the experimental investigation, a new two-dimensional 2-dof dynamic

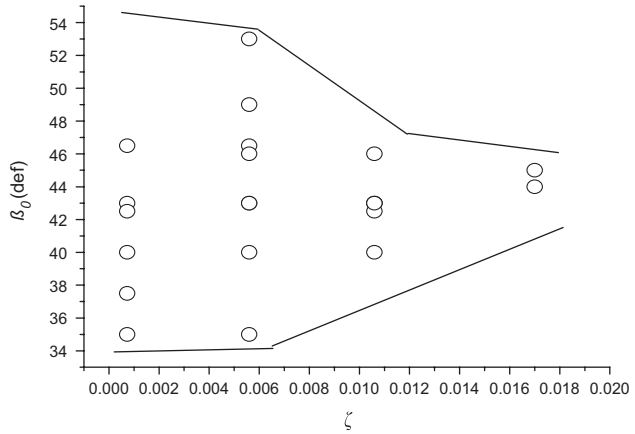

Fig. 9. Effect of damping on the unstable balance angle (experimental results).

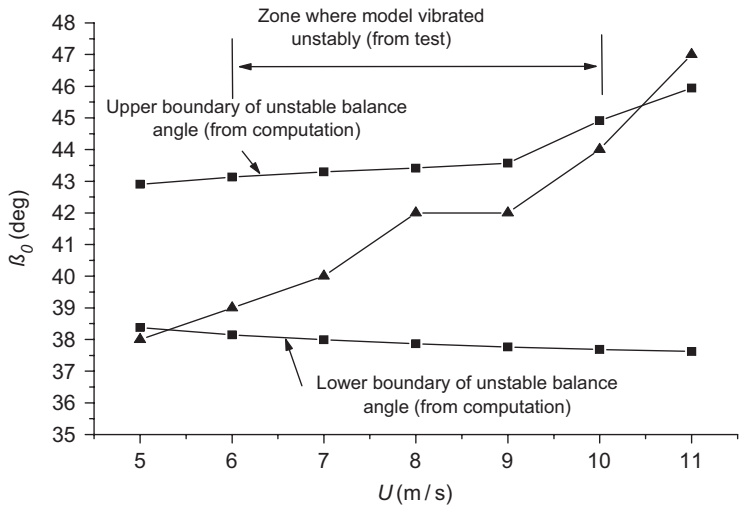

Fig. 10. Comparison of the theoretical and experimental results.

system, a cable model system with a movable artificial upper rivulet, was tested in a wind tunnel. Parametric studies were also undertaken to investigate the effects of major factors such as wind speed, frequency and damping of the cable, etc., on the unstable balance angle of the upper rivulet. The theoretical and experimental results matched well. The results from both the theoretical analysis and the wind tunnel test indicate that the zone of the unstable balance angle of the rivulet becomes small with an increase in frequency and damping, and becomes wide with increased wind speed. These research results might be valuable in explaining the mechanism for rain–wind induced vibration of stay cables.

Acknowledgments

The authors would like to gratefully acknowledge the support of the National Natural Science Foundation of China (50621062, 50178049).

References

Bosdogianni, A., Olivari, D., 1996. Wind- and rain-induced oscillations of cables of stayed bridges. Journal of Wind Engineering and Industrial Aerodynamics 64, 171–185.

Cao, D.Q., Tucker, R.W., Wang, C., 2003. A stochastic approach to cable dynamics with moving rivulets. Journal of Sound and Vibration 268, 291–304.

Cosentino, N., Flamand, O., Ceccoli, C., 2003. Rain–wind induced vibration of inclined stay cables, Part 1: experimental investigation and physical explanation. Wind and Structures 6, 471–484.

Du, X.Q., 2004. Theoretical and experimental studies on rain–wind induced vibration of stay cables in cable-stayed bridges. A Dissertation for Ph.D. Degree, Tongji University.

Flamand, O., 1995. Rain–wind induced vibration of cables. Journal of Wind Engineering and Industrial Aerodynamics 57, 353–362.

Geurts, C.P.W., Staalduinen, P.C.V., 1999. Estimation of the effects of rain–wind induced vibration in the design stage of inclined stay cables. In: Larsen, A., Larose, G.L., Livesey, F.M. (Eds.), Proceedings of the 10th International Conference on Wind Engineering. Copenhagen, Denmark, pp. 885–892.

Gu, M., Du, X.Q., 2005. Testing investigation for rain–wind induced vibration and its control of cables of cable-stayed bridges. Journal of Wind Engineering and Industrial Aerodynamics 93 (1), 79–95.

Gu, M., Lu, Q., 2001. Theoretical analysis of wind–rain induced vibration of cables of cable-stayed bridges. Journal of Wind Engineering and Industrial Aerodynamics 89, 125–128.

Gu, M., Liu, C.J., Lou, G.Q., Lin, Z.X., Xiang, H.F., 1998. Rain–wind induced vibration of cables on cable-stayed bridges and its control. Shanghai Journal of Mechanics 19 (4), 281–288 (in Chinese).

Gu, M., Liu, C.J., Xu, Y.L., Xiang, H.F., 2002. Response characteristics of wind excited cable with artificial rivulet. Applied Mathematics and Mechanics 23 (10), 1176–1187.

Hikami, Y., Shiraishi, N., 1988. Rain–wind induced vibrations of cables in cable stayed bridges. Journal of Wind Engineering and Industrial Aerodynamics 29, 409–418.

Main, J.A., Jones, N.P., 1999. Full scale measurements of stay cable vibration. In: Larsen, A., Larose, G.L., Livesey, F.M. (Eds.), Proceedings of the 10th International Conference on Wind Engineering. Copenhagen, Denmark, pp. 963–970.

Matsumoto, M., 1998. Observed behavior of prototype cable vibration and its generation mechanism. In: Larsen, Esdahl (Eds.), Bridge Aerodynamics. Balkema, Rotterdam, pp. 189–211.

Matsumoto, M., 2005. Motion-effect of water rivulet on rain–wind induced vibration of inclined stay-cables, in: Proceedings of the Sixth International Symposium on Cable Dynamics, pp. 255–262.

Matsumoto, M., Shirato, H., 2003. Field observation of the full scale wind-induced cable vibration. Journal of Wind Engineering and Industrial Aerodynamics 91, 13–26.

Matsumoto, M., Shirashi, N., Shirato, H., 1992. Rain–wind induced vibration of cables of cable-stayed bridges. Journal of Wind Engineering and Industrial Aerodynamics 41–42, 2011–2022.

Matsumoto, M., Saitoh, T., Kitazawa, M., Shirato, H., Nishizaki, T., 1995. Response characteristics of rain–wind induced vibration of stay-cables of cable-stayed bridges. Journal of Wind Engineering and Industrial Aerodynamics 57, 323–333.

Matsumoto, M., Yagi, T., Shigemura, Y., Tsusgima, D., 2001. Vortex-induced cable vibration of the cable-stayed bridges at high reduced wind velocity. Journal of Wind Engineering and Industrial Aerodynamics 89 (7–8), 633–647.

Matsumoto, M., Yagi, T., Sakai, S., Ohya, J., Okada, T., 2003. Aerostatic force/aerodynamic response characteristics of inclined/yawed cable. In: Proceedings of the 11th International Conference on Wind Engineering, Texas, USA, pp. 21–23

Ohshima, K., Nanjo, M., 1987. Aerodynamics stability of the cables of a cable-stayed bridge subject to rain (a case study of the Aji River Bridge). In: Proceedings of US-Japan Joint Seminar on Natural Resources, pp. 324–336

Pacheco, B.M., Fujino, Y., 1993. Keeping cables calm. Civil Engineering, ASCE 63, 56–58.

Persoon, A.J., Noorlander, K., 1999. Full scale measurements on the Erasmus bridge after rain/wind induced cable vibration. In: Larsen, A., Larose G.L., Livesey, F.M. (Eds.), Proceedings of the 10th International Conference on Wind Engineering, Copenhagen, Denmark, pp. 1019–1026.

Ruscheweyh, H.P., 1999. The mechanism of rain–wind-induced vibration. In: Larsen, Larose, Esdahl (Eds.), Wind Engineering into the 21st Century. Balkema, Rotterdam, pp. 1041–1047.

Shi, J.J., 2000. On countermeasures for mitigation of wind–rain induced vibration of cables of No.2 Nanjing Bridge over Yangtze River. Department of Bridge Engineering, Tongji University (in Chinese).

Verwiebe, C., Rucheweyh, H., 1998. Wind- and rain-induced oscillations of cable of cable-stayed bridge. Journal of Wind Engineering and Industrial Aerodynamics, 1005–1013.

Wilde, K., Witkowski, W., 2003. Simple model for rain–wind induced vibrations of stayed cables. Journal of Wind Engineering and Industrial Aerodynamics 91, 873–891.

Xu, Y.L., Wang, L.Y., 2003a. Analytical study of wind–rain-induced cable vibration. Journal of Wind Engineering and Industrial Aerodynamics 91, 27–40.

Xu, Y.L., Wang, L.Y., 2003b. Analytical study of wind–rain-induced cable vibration: SDOF model. Journal of Wind Engineering and Industrial Aerodynamics 91, 27–40.

Yamaguchi, H., 1990. Analytical study on growth mechanism of rain vibration of cables. Journal of Wind Engineering and Industrial Aerodynamics 33, 73–80.

Zuo, D., Jones, N.P., Main, J.A., 2004. Vortex- and rain–wind-induced stay cable vibrations in a three-dimensional environment, in: Proceedings of the Fifth International Colloquium on Bluff Body Aerodynamics and Applications. Ottawa, Canada, pp. 397–400.